Chapter 14

[2]Pseudorotaxanes Based on the Cryptand/Monopyridinium Recognition Motif

14.1. INTRODUCUTION

Threaded structures, such as pseudorotaxanes, rotaxanes, catenanes, polypseudorotaxanes, polyrotaxanes, and polycatenanes, have been widely studied due to not only their topological importance but also their potential applications.[1] Up to now, the main host-guest recognition motifs used for fabrication of these threaded structures are bis(*p*-phenylene)-34-crown-10/paraquat,[2] crown ether/secondary ammonium salts,[3] benzylic tetraamide macrocycle/amides or phenolates,[4] cyclic bisparaquat/electron-rich aromatics,[5] cyclodextrins/hydrophobic compounds,[6] calixarene/paraquat,[7] cryptand/paraquat,[8] dibenzo-24-crown-8/1,2-bis(4,4'-bipyridinium)ethane salts,[9] and cucurbituril/paraquat or secondary ammonium salts.[10] These recognition motifs are mainly based on hydrogen bonding, π-π stacking, charge transfer, and hydrophilic-hydrophobic interactions. Metal-ligand coordinations have also been widely used in the preparation of threaded structures.[11]

The first cryptand was reported in 1968.[12a] The original objective for preparing cryptands was to strongly bind metal ions and small organic molecules by encapsulation.[12] Recently progress has been made in synthesis of cryptands and supramolecular cryptands[13] that can complex large organic guests, such as paraquat derivatives and bis(secondary ammonium) salts. We reported very strong complexations between a cryptand and paraquat derivatives in 1999.[8d] Later, we reported cooperative complexation between a cryptand and a bisparaquat derivative,[8e] two pseudorotaxane-

like inclusion cryptand/paraquat [3]complexes,[8f] and the formation of dimers of inclusion cryptand/paraquat complexes driven by dipole-dipole and face-to-face π-stacking interactions.[8g] Specifically, a bis(*m*-phenylene)-32-crown-10 based diester cryptand with a pyridyl nitrogen atom located at a site occupied by either water or a PF_6 anion in analogous crown ether based complexes exhibited a very high association constant K_a = 5.0×10^6 M^{-1} in acetone with paraquat, 9000 times greater than the crown ether system.[8h] We also found that the formation of supramolecular cryptands by chelation of difunctional macrocycles can improve the complexations with paraquat derivatives,[14a] a bis(secondary ammonium) salt,[14b] and a bisparaquat derivative.[14c] These cryptands and supramolecular cryptands have proven to be much better hosts for organic guests than corresponding simple crown ethers.[8,14] Cryptands have also been used in the binding of inorganic anions,[15] anionic colorimetric dyes,[15] acetic acid,[16] and ion-pairs.[17]

Simple monopyridinium salts have been widely studied in chemistry not only due to their easy availability but also because of their potential applications.[18] For the most recent examples, they have been used in the synthesis of novel monomeric and homodimeric cyanine dyes for nucleic acid detection,[18e] preparation of cationic lipids in gene delivery,[18f] fabrication of novel stilbazolium analogues as second-order nonlinear optical materials,[18g] and manufacture of amperometric sensors.[18h] However, monopyridinium salts have been rarely used in preparation of threaded structures. A few examples are the Beer systems based on ion-pair recognition by ditopic hosts.[19]

Here we report the first cryptand/monopyridinium [2]pseudorotaxanes, which are based on the new cryptand/monopyridinium recognition motif. The formation of these pseudorotaxanes is mainly driven by hydrogen bonding and face-to-face π-stacking interactions.

14.2. RESULTS AND DISCUSSION

A. Design of Cryptand/Monopyridinium [2]Pseudorotaxanes.

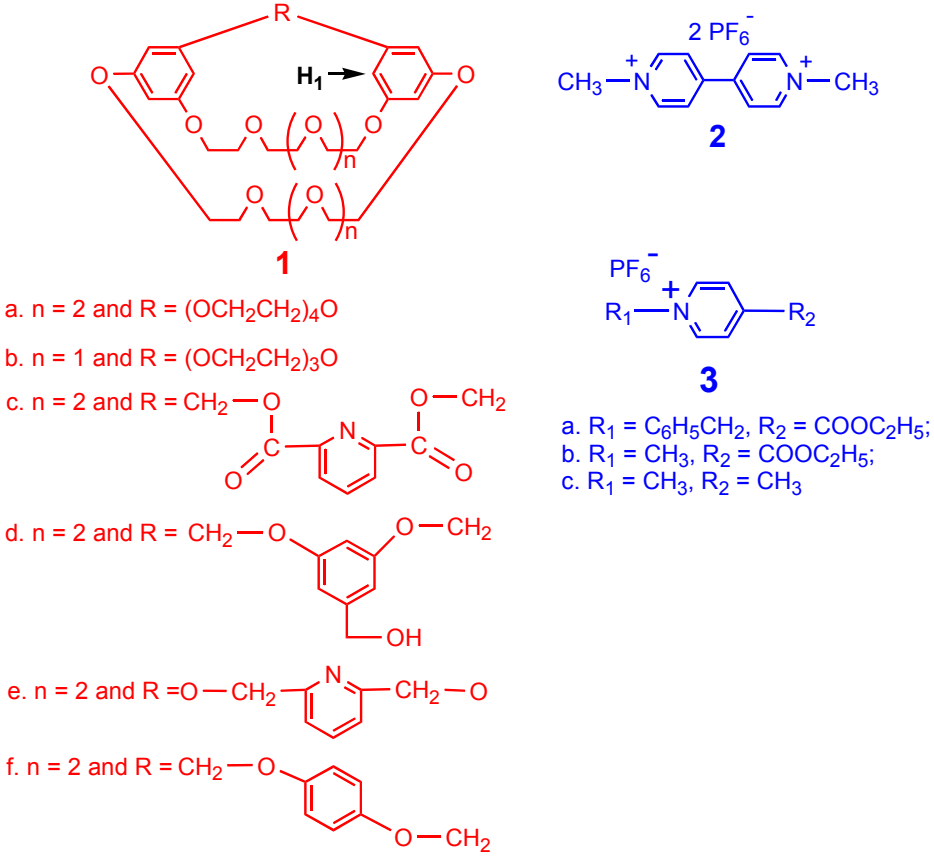

The design of these cryptand/monopyridinium [2]pseudorotaxanes was inspired by the formation of two 2:1 psueodorotaxane-like cryptand/paraquat [3]complexes (Figure 1).[8f] On the basis of these structures in which each paraquat unit is shared by two cryptand moieties, we theorized that these cryptands[8d,f,h] should be able to complex monopyridinium derivatives. The folded complexes of monopyridinium salts and crown ethers reported by Lämsä et al.[20] also piqued our interest. Therefore, monopyridinium derivatives **3** were prepared and their complexation with cryptands **1** was studied.

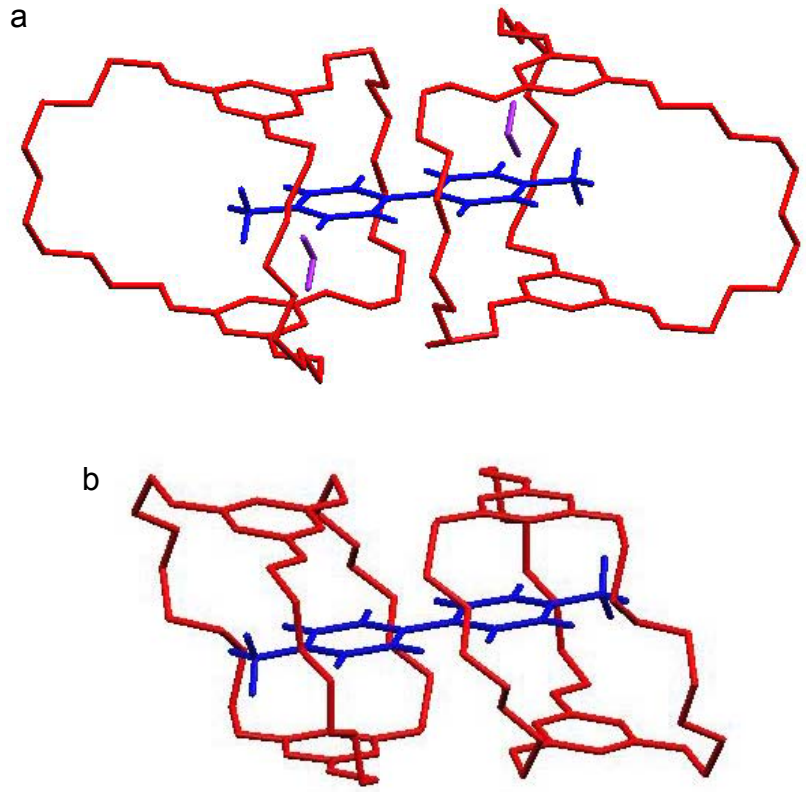

Figure 1. X-ray structures of **1a•2•1a•**$2H_2O$ (a) and **1b•2•1b** (b).[8f]

B. Syntheses of Cryptand Hosts and Monopyridinium Guests.

The preparation of bis(*m*-phenylene)-32-crown-10 or bis(*m*-phenylene)-26-crown-8 based cryptand hosts **1** followed previously reported procedures.[8d,f,h] Monopyridinium salts **3a** and **3b** were made by the reaction of excess ethyl isonicotinate with a bromide or iodide followed by ion exchange with ammonium hexafluorophosphate. Monopyridinium salt **3c** was synthesized according to a reported method.[21] All these monopyridinium salts were purified by recrystallization in deionized water and dried under vacuum at 100 °C.

C. Complexation of Cryptand Hosts 1 with Monopyridinium Salts 3.

The yellow color of solutions of these cryptands with monopyridinium derivatives is not as intense as that of solutions of these cryptands with paraquat derivatives.[8d,f-h] This indicates that charge transfer between the cryptands and the monopyridinium derivatives is weaker than that between cryptands and paraquat derivatives. A Job plot[22] (Figure 2) based on proton NMR data demonstrated that the complex between **1a** and **3a** was of 1:1 stoichiometry in acetone solution. In the same way, it was found that other complexes between **1** and **3** also had 1:1 stoichiometry in solution.

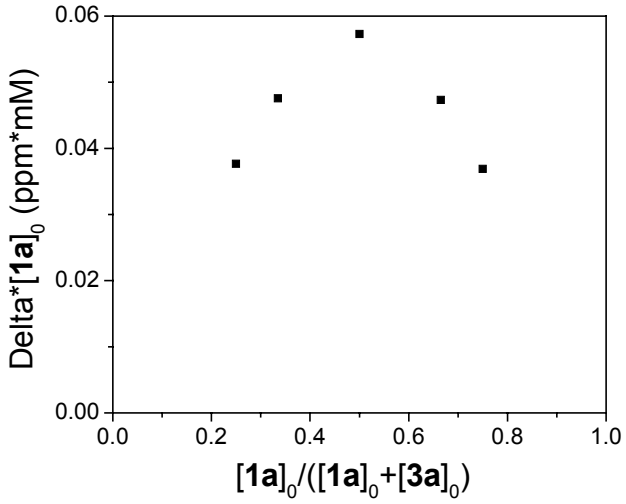

Figure 2. Job plot showing the 1:1 stoichiometry of the complex between **1a** and **3a** in [D_6]acetone. [**1a**]$_0$ + [**3a**]$_0$ = 2.00 mM**.** [**1a**]$_0$ and [**3a**]$_0$ are initial concentrations of **1a** and **3a**. Delta = chemical shift change for H_1 of **1a**.

Three solutions containing **1a**, **3a**, and equimolar **1a** and **3a** were characterized by proton NMR in 1:1 acetone:chloroform (Figure 3). These NMR spectra indicated that exchange was fast and complexation was relatively strong on the basis of the significant upfield shifts of the pyridinium protons (H_6 and H_7) of guest **3a**, the aromatic protons (H_1), and α-ethyleneoxy protons (H_2) of host **1a**. Furthermore, benzylic protons (H_8) of

3a and β-ethyleneoxy protons (H_4) of **1a** move upfield, while phenyl and ester methylene protons (H_9, H_{10}, and H_5) of **3a** and ethyleneoxy protons H_3 of **1a** move downfield.

The association constants (K_a) for these cryptand/monopyridinium complexes were determined (Tables 1 and 2). Monopyridinium salt **3a** appears to be a slightly better guest for **1a** than **3b** (Table 1), indicating that the N-benzyl group is better for complexation than the N-methyl group. This agrees with the fact that a phenylene ring is more electron-withdrawing than a proton. The complex **1a•3c** also has a higher association constant than the complex **1a•3b** (Table 1), indicating that the methyl group at the 4-position of the pyridinium ring is better for complexation than the ester group at the same position. The substitution of the methyl group for the ester group at the 4-position has two effects. On one hand, the ester group is more electron-withdrawing than the methyl group; this makes the pyridinium ring more electron-poor and thus increases charge transfer interactions between the cryptand host and the monopyridinium guest. On the other hand, the methyl protons are acidic and provide binding sites. Obviously here the second effect is more important.

The balance of the substituent effects at the pyridyl nitrogen atom and at the 4-position leads to complexes **1a•3a** and **1a•3c** with similar K_a values. All three complexes of **1a** have about 1.5 times higher association constants in 1:1 acetone:chloroform than in acetone (Table 1) because of the decrease of the solvent polarity.

The K_a value of the complex **1a•3a** of the larger 32-crown-10-based cryptand **1a** is about four times of that of the complex **1b•3a** of the smaller 26-crown-8-based cryptand **1b** (Table 2). In the ethyleneoxy bridges of the cryptands, the aliphatic oxygen atoms are more basic than the phenolic oxygen atoms because of p-π conjugation in the latter; since there are more aliphatic oxygen atoms in **1a** (9) than in **1b** (6) it is understandable that K_a is larger for **1a•3a** than **1b•3a**, as also observed in the case of **1a•2** and **1b•2**.[8f]

The ratio of K_a values corresponding to **1b•3a**, **1d•3a**, **1e•3a**, **1a•3a**, **1f•3a**, and **1c•3a** is 1.0:2.4:3.0:4.0:9.3:130 (Table 2), so obviously here **1c** is the best cryptand host for monopyridinium salts **3**. The small increase in association constant from **1d•3a** to **1e•3a** is the result of the introduction of an additional binding site, the pyridyl nitrogen

atom, on the third bridge. The notable 30-fold increase in association constant from **1a•3a** to **1c•3a** is due to the introduction of a better binding site, the pyridyl nitrogen atom, just as we have seen in complexation studies between these cryptands and paraquat derivatives.[8d,f,h] These interactions were confirmed by the X-ray analyses below.

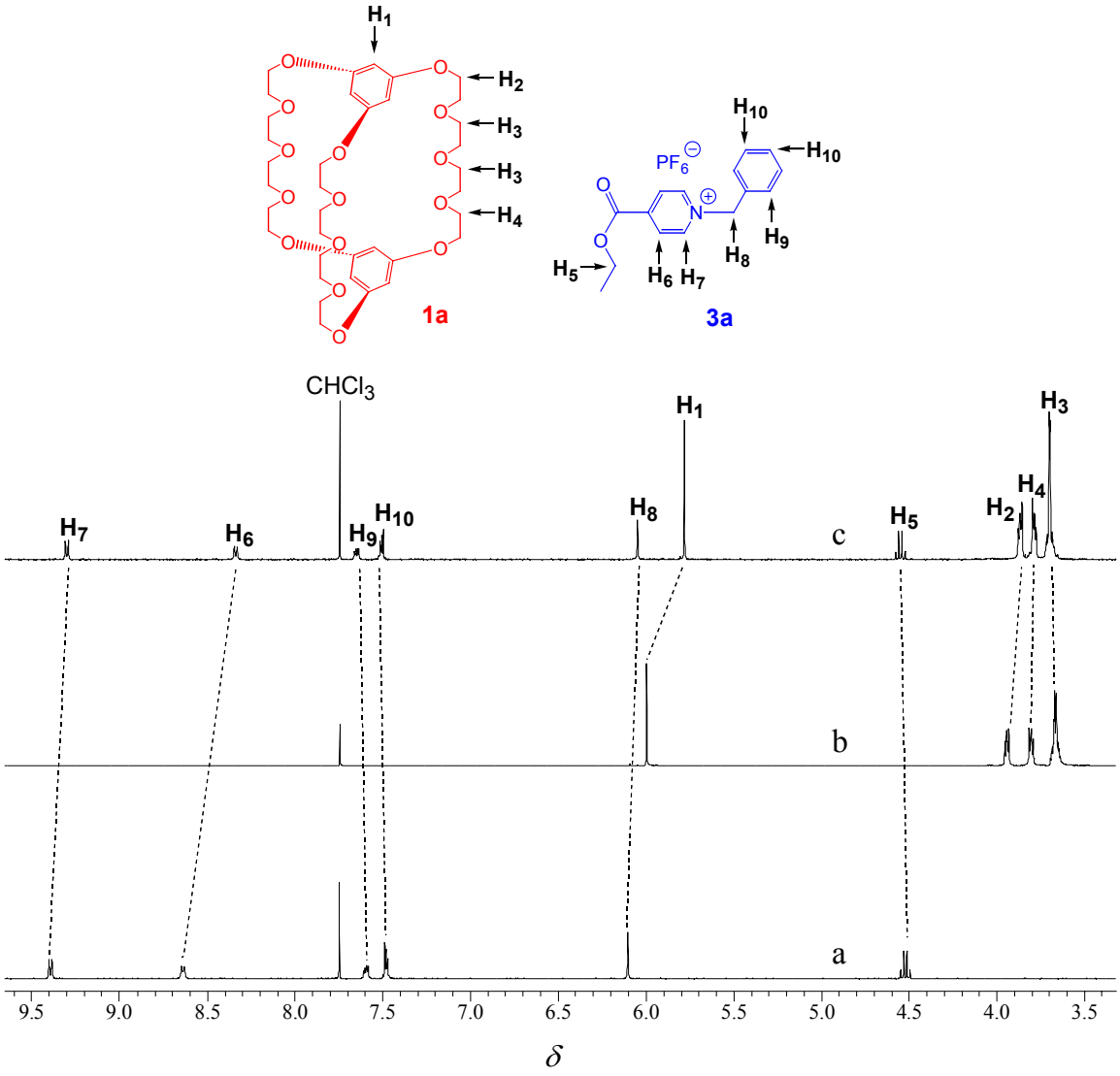

Figure 3. Partial proton NMR spectra (400 MHz, 1:1 $CDCl_3$:CD_3COCD_3, 22 °C) of monopyridinium salt **3a** (a, bottom), cryptand **1a** (b, middle), and 3.00 mM **1a** and **3a** (c, top).

Table 1. Association Constants (K_a) Values (M^{-1}) in Different Solvents for **1a**/Monopyridinium Complexes at 22 °C.

Solvent	**1a•3a**	**1a•3b**	**1a•3c**
acetone	182 ± 20	173 ± 40	193 ± 31
1:1 acetone:chloroform	588 ± 60	426 ± 59	536 ± 48

Table 2. Association Constants (K_a) Values (M^{-1}) for Cryptand/**3a** Complexes at 22 °C.

Solvent	**1a•3a**	**1b•3a**	**1c•3a**	**1d•3a**	**1e•3a**	**1f•3a**
1:1 acetone:chloroform	588 ± 60	141 ± 21	18.6 (± 2.0) × 10^3	332 ± 33	423 ± 42	1.31 (± 0.12) × 10^3

D. Electrospray Ionization Mass Spectrometric Characterization of Cryptand/Monopyridinium [2]Pseudorotaxanes.

Some of these cryptand/monopyridinium complexes were characterized by electrospray ionization mass spectrometry and their 1:1 stoichiometries were confirmed (Table 3, See Supporting Information for more details). The mass spectrum for **1a•3a** is given in Figure 4 as an example. No peaks related to other stoichiometries were found.

Table 3. Observed Mass/Charge Ratios for 1:1 Cryptand/Monopyridinium Complexes in $CH_3CN/CHCl_3$ (4:1) from Electrospray Ionization Mass Spectrometric Characterization.

Complex	**1•3** + Na	**1•3** + Li – $HOCH_2CH_2OH$	**1•3** – PF_6
1a•3a[a]	1136.4 (10%)	1058.8 (10%)	968.7 (100%)
1a•3b[b]	1060.5 (6%)	982.6 (7%)	892.6 (100%)
1a•3c	1002.6 (1%)	924.8 (8%)	834.6 (100%)
1c•3a[c]	1137.4 (5%)		969.3 (64%)
1d•3a[d]			942.5 (43%)
1e•3a[d,e]			913.4 (28%)

[a] One more peak was found for **1a•3a**: *m*/*z* 892.7 [**1a•3a** – PF_6 – C_6H_5 + H]$^+$ (6%). [b] One more peak was found for **1a•3b**: *m*/*z* 864.6 [**1a•3b** – PF_6 – C_2H_4]$^+$ (14%). [c] Four more peaks were found for **1c•3a**: *m*/*z* 1123.3 [**1c•3a** + Na – CH_3 + H]$^+$ (4%), 955.3 [**1c•3a** – PF_6 – CH_3 + H]$^+$ (100%), 912.3 [**1c•3a** – HPF_6 – C_6H_6 + Na – H]$^+$ (24%), and 898.3 [**1c•3a** – PF_6 – C_6H_6 + Li]$^+$ (29%). [d] The base peak was at *m*/*z* 242.2, corresponding to [**3a** – PF_6]$^+$. [e] One more peak was found for **1e•3a**: *m*/*z* 1059.4 [**1e•3a** + H]$^+$ (1%).

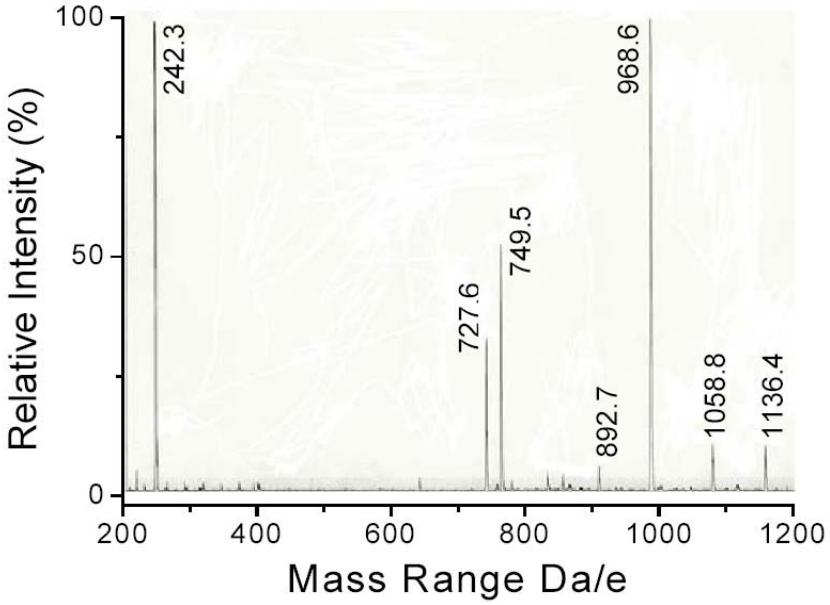

Figure 4. Electrospray mass spectrum of a solution of **1a** and **3a** in a mixture of acetonitrile and chloroform (4:1). Assignments of main peaks: *m/z* 1136.4 [**1a•3a** + Na]$^+$, 1058.8 [**1a•3a** + Li – $HOCH_2CH_2OH$]$^+$, 968.6 [**1a•3a** – PF_6]$^+$, 892.7 [**1a•3a** – PF_6 – C_6H_5 + H]$^+$, 749.5 [**1a** + Na]$^+$, 727.6 [**1a** + H]$^+$, and 242.3 [**3a** – PF_6]$^+$.

E. Solid State Structures of [2]Pseudorotaxanes 1a•3a and 1c•3a.

X-ray analyses were done on yellow crystals of **1a•3a** and colorless crystals of **1c•3a** grown by vapor diffusion of pentane into equimolar acetone solutions of the corresponding cryptand and monopyridinium salt. These crystal structures (Figures 5 and 6) demonstrated that these complexes are [2]pseudorotaxanes. For both **1a•3a** and **1c•3a**, the main stabilization interactions are hydrogen bonding and face-to-face π-stacking interactions in the solid state. Two methylene hydrogens on the ethyl ester group and an α-pyridinium hydrogen of **3a** are involved in hydrogen bonding (**D**, **E**, **F** of Figure 5; **I**, **J**, and **K** of Figure 6) with oxygen atoms on ethyleneoxy chains of the cryptand hosts. The two β-pyridinium hydrogens of **3a** are not involved in interactions with the cryptand hosts. The pyridinium ring of **3a** nicely lies at the mid-point between the two phenylene rings of the cryptand hosts, presumably in order to maximize face-to-face π-stacking.

However, there are some differences. First, the left α-pyridinium hydrogen of **3a** is connected to cryptand **1a** indirectly by a water bridge (**A**, **B**, and **C** of Figure 5), while this left α-pyridinium hydrogen of **3a** is connected to **1c** directly by a hydrogen bond (**H** of Figure 6) to the pyridyl nitrogen atom on the host, whose third bridge is shorter (9 atoms) than that of **1a** (13 atoms). Second, one benzylic hydrogen of **3a** is involved in hydrogen bonding between the host and guest in **1a•3a** (**G** of Figure 5), while neither of them are involved in hydrogen bonding to the host in **1c•3a** (Figure 6). Third, the centroid-centroid distance between the phenylene rings of the cryptand host in **1a•3a** is 6.88 Å, while this distance is 6.98 Å in **1c•3a**. This is presumably due in part to the shorter (9 atoms in **1c** vs. 13 atoms in **1a**) and more rigid third arm of **1c**, which pushes the phenylene rings apart. This difference is consistent with the fact that charge transfer interactions between the host and guest in **1a•3a** are stronger than those in **1c•3a**; the crystals **1a•3a** of are yellow, while the crystals of **1c•3a** are colorless.

The ^{1}H NMR chemical shift changes of host **1a** upon complexation are consistent with a structure in solution similar to that of **1a•3a** in the solid state (Figure 5). Protons H_1, H_2 and H_4 are in shielding regions of the pyridinium or terminal phenylene ring of the guest **3a**, while H_3 resides in the deshielding environment of both the pyridinium and terminal phenylene rings of the guest **3a**. The downfield shift of the ethyl ester methylene (H_5) and phenylene protons (H_9 and H_{10}) of the guest **3a** is consistent with their positions in the deshielding region of the aromatic moieties of the cryptand host **1a**. The upfield shift of the pyridinium (H_6 and H_7) and benzylic protons (H_8) of the guest **3a** is consistent with their positions in the shielding region of the aromatic moieties of the cryptand host **1a**.

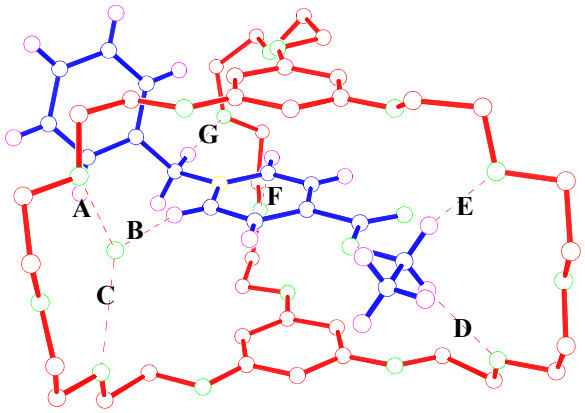

Figure 5. Ball-stick view of one unique host-guest complex (the other is similar) in the X-ray structure of **1a•3a**. **1a** is red, **3a** is blue, and the water molecule is green. The PF_6 counterion, other solvent molecules, and the hydrogens on **1a** were omitted for clarity. Oxygens are green, nitrogens are yellow, and hydrogens are magenta. Hydrogen-bond parameters: C(O)···O distances (Å), H···O distances (Å), C(O)-H···O angles (deg) **A**, 2.89, not available, not available; **B**, 3.13, 2.30, 146; **C**, 2.87, not available, not available; **D**, 3.26, 2.33, 157; **E**, 3.33, 2.51, 140, **F**, 3.18, 2.60, 120; **G**, 3.34, 2.35, 175. Face-to-face π-stacking parameters: centroid-centroid distances (Å) 3.83, 3.83; ring plane/ring plane inclinations (deg): 3.8, 1.4.

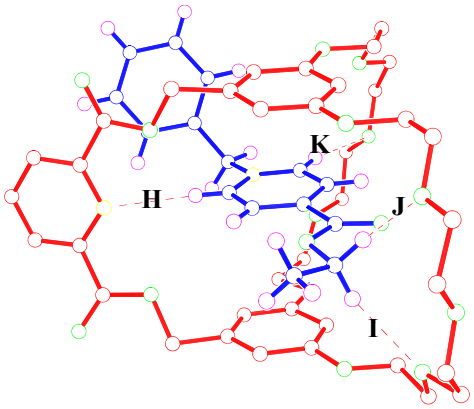

Figure 6. Ball-stick view of the X-ray structure of **1c•3a**. **1c** is red and **3a** is blue. The PF_6 counterion, solvent molecules, and the hydrogens on **1c** were omitted for clarity. Oxygens are green, nitrogens are yellow, and hydrogens are magenta. Hydrogen-bond parameters: C···O(N) distances (Å), H···O(N) distances (Å), C-H···O(N) angles (deg) **H**, 3.61, 2.78, 149; **I**, 3.41, 2.49, 157; **J**, 3.28, 2.37, 154; **K**, 3.57, 2.65, 168. Face-to-face π-stacking parameters: centroid-centroid distances (Å) 3.91, 3.91; ring plane/ring plane inclinations (deg): 6.1, 3.5.

F. Solid State Structures of Cryptand 1b and [2]Pseudorotaxane 1b•3a.

Colorless crystals of cryptand **1b** were grown by slow evaporation of an acetone solution of **1b**, while yellow crystals of [2]pseudrotaxane **1b•3a** were grown by vapor diffusion of pentane into equimolar acetone solutions of cryptand **1b** and monopyridinium salt **3a**. The X-ray crystal structures of **1b** and **1b•3a** are shown in Figure 7. The two phenylene rings of **1b** are not parallel to each other but exhibit a twist angle of 20° (Figure 7a). The centroid-centroid distance between them is 4.78 Å. Comparison of the crystal structures of **1b** and **1b•3a** (Figures 7a and 7b) shows that the conformation of the cryptand host **1b** does not change much during complexation because of its preorganization. However, the twist angle and centroid-centroid distance between two phenylene rings of **1b** are changed to 6.2° and 6.37 Å respectively due to the threading of the monopyridinium guest **3a** through its cavity. Similar to the crystal structures of the above two bis(*m*-phenylene)-32-crown-10 based cryptand/monopyridnium [2]pseudrotaxanes **1a•3a** (Figure 5) and **1c•3a** (Figure 6), the

bis(*m*-phenylene)-26-crown-8 based cryptand/monopyridnium complex **1b•3a** is also a [2]pseudorotaxane, it is also stabilized by hydrogen bonding and face-to-face π-stacking interactions in the solid state, the two β-pyridinium hydrogens of **3a** are not involved in interactions with the cryptand host, and the pyridinium ring of **3a** nicely lies at the mid-point between the two phenylene rings of **1b**. However, at least two differences can be observed. First, both α-pyridinium hydrogen atoms of **3a** are connected to the cryptand host by only one hydrogen bond in **1a•3a** and **1c•3a**, while one α-pyridinium hydrogen of **3a** is connected to cryptand **1b** by two hydrogen bonds (**L** and **M** of Figure 7) and the other α-pyridinium hydrogen atom is connected to **1b** by one hydrogen bond (**O** of Figure 7). Second, both methylene hydrogen atoms on the ethyl ester group of **3a** are connected to the cryptand host by hydrogen bonds in **1a•3a** and **1c•3a**, while only one methylene hydrogen atom on the ethyl ester group of **3a** is connected to cryptand **1b** by a hydrogen bond (**N** of Figure 7).

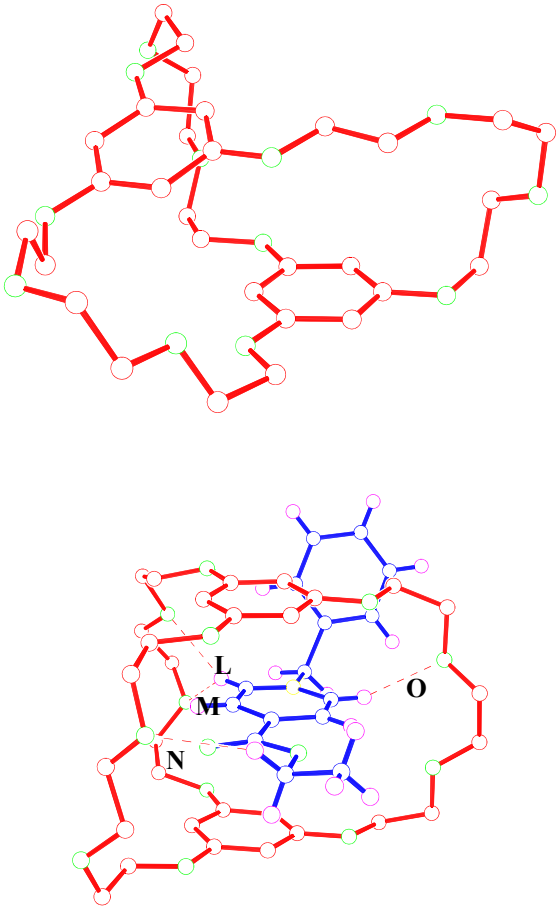

Figure 7. Ball-stick view of the X-ray structures of cryptand **1b** (a) and [2]pseudorotaxane **1b•3a** (b). **1b** is red and **3a** is blue. The PF_6 counterion, solvent molecules, and the hydrogens on **1b** were omitted for clarity. Oxygens are green, nitrogens are yellow, and hydrogens are magenta. Hydrogen-bond parameters: C···O distances (Å), H···O distances (Å), C-H···O angles (deg) **L**, 3.32, 2.48, 148; **M**, 3.15, 2.36, 141; **N**, 3.48, 2.58, 151; **O**, 3.26, 2.59, 128. Face-to-face π-stacking parameters: centroid-centroid distances (Å) 3.51, 3.51; ring plane/ring plane inclinations (deg): 0.8, 5.7.

G. Solid State Structures of [2]Pseudorotaxane 1d•3a.

It is interesting that two different types of yellow crystals of **1d•3a** were obtained by vapor diffusion of pentane into acetone solutions of the components. Therefore, two different X-ray structures (Figures 8a and 8b), in which complex **1d•3a** has different co-conformations, were obtained. This is possibly due to the flexibility of the ethyl ester group at 4-position of the pyridinium ring of guest **3a**. For both crystal structures, complex **1d•3a** is a pseudorotaxane, the main stabilization interactions are hydrogen bonding and face-to-face π-stacking interactions in the solid state, and there are hydrogen bonds that involve methylene hydrogens on the ethyl ester group of **3a** (**S**, **T**, **V**, and **W** of Figure 8). There are at least two points that are worth of noting in comparison with the above three pseudorotaxane crystal structures. First, one benzylic hydrogen of **3a** is involved in hydrogen bonding between the host and guest in **1a•3a** (**G** of Figure 5) and one of the two crystal structures of **1d•3a** (**Q** of Figure 8a), while neither of them are involved in hydrogen bonding to the host in **1b•3a** (Figure 7), **1c•3a** (Figure 6), and the other crystal structure of **1d•3a** (Figure 8b). Second, the pyridinium ring of **3a** nicely lies at the mid-point between the two phenylene rings of the cryptand host in **1a•3a** (Figure 5), **1b•3a** (Figure 7) and **1c•3a** (Figure 6), while the distances between the pyridinium ring of **3a** and the two phenylene rings of the cryptand host are not equal to each other in the two crystal structures of **1d•3a** (Figures 8a and 8b). A possible reason for this is that hydrogen bonding is more important than face-to-face π-stacking interactions for this complex, so the three aromatic rings are placed in this way to maximize hydrogen bonding.

There are at least five major differences in the two crystal structures of **1d•3a**. First, the most important difference is that the monopyridinium guest **3a** is threaded through the cavity of the 32-crown-10 part of the cryptand host in one crystal structure (Figure 8a), while the 32-crown-10 part forms a taco complex conformation with the monopyridinium guest in the other (Figure 8b). Second, none of the hydrogens on the terminal phenylene ring of **3a** are involved in hydrogen bonding between the cryptand host and the monopyridinium guest in one crystal structure of **1d•3a** (Figure 8a) [and even in all above pseudorotaxane crystal structures (Figures 5, 6, and 7)], while there are

two hydrogen bonds, which involve two different hydrogens on the terminal phenylene ring of **3a**, in the other crystal structure of **1d•3a** (**U** and **Y** of Figure 8b). Third, one benzylic hydrogen of **3a** is involved in hydrogen bonding between the host and guest in one crystal structure of **1d•3a** (**Q** of Figure 8a), while neither of them is involved in hydrogen bonding to the host in the other (Figure 8b). Fourth, there are two hydrogen bonds between the host and guest based on one α-pyridinium hydrogen of **3a** in one crystal structure of **1d•3a** (**P** and **R** of Figure 8a), while there is only one of this type of hydrogen bond in the other (**X** of Figure 8b). Fifth, there is an edge-to-face π-stacking interaction between the pyridinium ring of **3a** and the phenylene ring of the third bridge of **1d** in one crystal structure (Figure 8b) but not in the other (Figure 8a) [and even in all above pseudorotaxane crystal structures (Figures 5, 6, and 7)]. Edge-to-face π-stacking interactions were observed before in our studies of crown ether/bis(secondary ammonium) complexes.[3b,c]

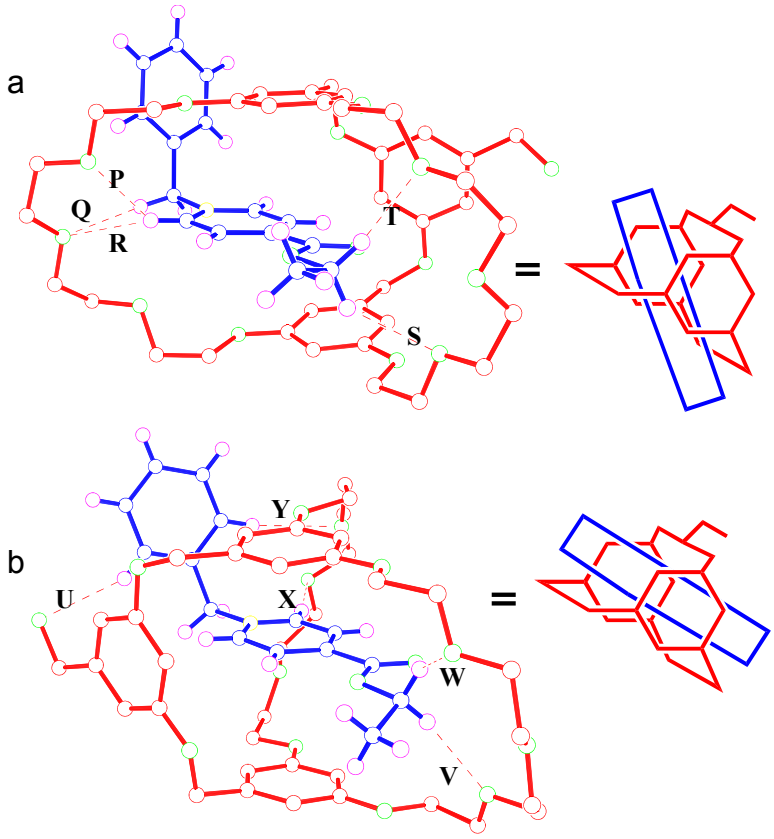

Figure 8. Ball-stick view of the X-ray structures of dimorphic forms of **1d•3a**. **1d** is red and **3a** is blue. The PF_6 counterion, solvent molecules, and the hydrogens on **1d** were omitted for clarity. Oxygens are green, nitrogens are yellow, and hydrogens are magenta. (a) Hydrogen-bond parameters: C···O(N) distances (Å), H···O(N) distances (Å), C-H···O(N) angles (deg) **P**, 3.17, 2.44, 134; **Q**, 3.56, 2.64, 156; **R**, 3.38, 2.51, 153; **S**, 3.49, 2.66, 141; **T**, 3.34, 2.42, 153. Face-to-face π-stacking parameters: centroid-centroid distances (Å) 3.68, 4.29; ring plane/ring plane inclinations (deg): 5.9, 12.2. (b) Hydrogen-bond parameters: C···O(N) distances (Å), H···O(N) distances (Å), C-H···O(N) angles (deg) **U**, 3.49, 2.63, 153; **V**, 3.24, 2.34, 153; **W**, 3.27, 2.57, 128; **X**, 3.22, 2.29, 172; **Y**, 3.40, 2.53, 155. Face-to-face π-stacking parameters: centroid-centroid distances (Å) 4.20, 3.98; ring plane/ring plane inclinations (deg): 5.8, 3.2. Edge-to-face π-stacking parameters: hydrogen-centroid distance (Å) 2.51, carbon-centroid distance (Å) 3.38, carbon-hydrogen-centroid angle (deg): 155.

H. Solid State Structure of [2]Pseudorotaxane 1e•3a.

Pale yellow crystals of [2]pseudrotaxane **1e•3a** were grown by vapor diffusion of pentane into acetone solutions of monopyridinium salt **3a** and excess cryptand **1e**. The X-ray crystal structure of **1e•3a** is shown in Figure 9. Similar to the crystal structures of the above four cryptand/monopyridnium [2]pseudrotaxanes (Figures 5-8), bis(*m*-phenylene)-32-crown-10 based cryptand/monopyridnium complex **1e•3a** is also a [2]pseudorotaxane and it is also stabilized by hydrogen bonding and face-to-face π-stacking interactions in the solid state. However, there are three points that are worth mentioning. First, what is unique here is that one β-pyridinium hydrogen of **3a** is involved in hydrogen bonding (**B1** of Figure 9) to the pyridyl atom of cryptand **1e**, while neither of two β-pyridinium hydrogens of **3a** is involved in hydrogen bonding with the cryptand host in the crystal structures of all above cryptand/monopyridnium [2]pseudrotaxanes (Figures 5, 6, 7, and 8). Second, one methylene hydrogen atom on the ethyl ester group of **3a** is involved in two hydrogen bonds (**C1** and **D1** in Figure 9) and the other is not involved in any hydrogen bonding to the cryptand host in **1e•3a**, while both methylene hydrogen atoms on the ethyl ester group of **3a** are connected to the cryptand host by one hydrogen bond in all above bis(*m*-phenylene)-32-crown-10 based cryptand/monopyridnium [2]pseudrotaxanes (Figures 5, 6, and 8). Third, both α-pyridinium hydrogens of **3a** are connected to the cryptand host directly or indirectly by at least a hydrogen bond in the crystal structures of cryptand/monopyridnium [2]pseudrotaxanes **1a•3a** (**A**, **B**, **C**, and **F** in Figure 5), **1c•3a** (**H** and **K** in Figure 6), and **1b•3a** (**L**, **M**, and **O** in Figure 7), while only one α-pyridinium hydrogen of **3a** is involved in hydrogen bonding to the cryptand host in **1d•3a** (**P** and **R** in Figure 8a and **X** in Figure 8b) and **1e•3a** (**Z** and **A1** in Figure 9) in the solid state.

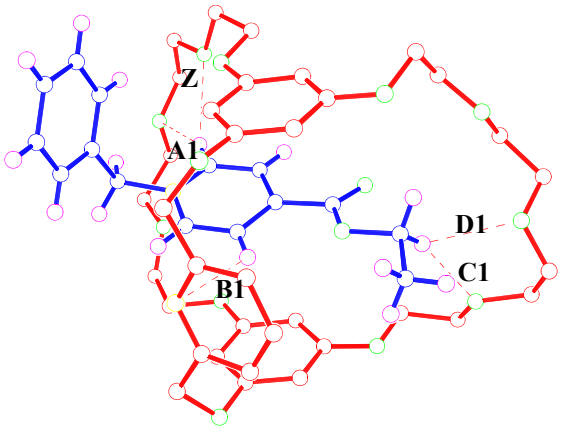

Figure 9. Ball-stick view of [2]pseudorotaxane **1e•3a**. **1e** is red and **3a** is blue. The PF_6 counterion, solvent molecules, and the hydrogens on **1e** were omitted for clarity. Oxygens are green, nitrogens are yellow, and hydrogens are magenta. Hydrogen-bond parameters: C···O distances (Å), H···O distances (Å), C-H···O angles (deg) **Z**, 3.11, 2.45, 127; **A1**, 3.25, 2.35, 159; **B1**, 3.36, 2.73, 125; **C1**, 3.27, 2.36, 153; **D1**, 2.99, 2.50, 111. Face-to-face π-stacking parameters: centroid-centroid distances (Å) 4.05, 4.18; ring plane/ring plane inclinations (deg): 10.6, 10.3.

I. Solid State Structure of [2]Pseudorotaxane 1f•3a.

Pale yellow crystals of [2]pseudrotaxane **1f•3a** were grown by vapor diffusion of pentane into acetone solutions of monopyridinium salt **3a** and excess cryptand **1f**. The X-ray crystal structure of **1f•3a** is shown in Figure 10. Similar to the crystal structures of the above five cryptand/monopyridnium [2]pseudrotaxanes (Figures 5-9), complex **1f•3a** is also a [2]pseudorotaxane and it is also stabilized by hydrogen bonding and face-to-face π-stacking interactions in the solid state. The crystal structure (Figure 10) of **1f•3a** is the same as one crystal structure (Figure 8a) of **1d•3a** in terms of which hydrogen atoms are involved in how many hydrogen bonds to the cryptand host. That is to say, for both of them, one benzylic hydrogen is involved in a hydrogen bond (**Q** in Figure 8a and **G1** in Figure 10), one α-pyridinium hydrogen is involved in two hydrogen bonds (**P** and **R** in Figure 8a and **H1** and **I1** in Figure 10), and both methylene hydrogen atoms on the ethyl ester group are involved in hydrogen bonding (**S** and **T** in Figure 8a and **E1** and **F1** in Figure 10) between the cryptand host and monopyridinium guest. Similar to the other

crystal structure of **1d•3a** (Figure 8b), **1f•3a** was also stabilized by an edge-to-face π-stacking interaction between the pyridinium ring of **3a** and the phenylene ring on the third bridge of the cryptand host (Figure 10).

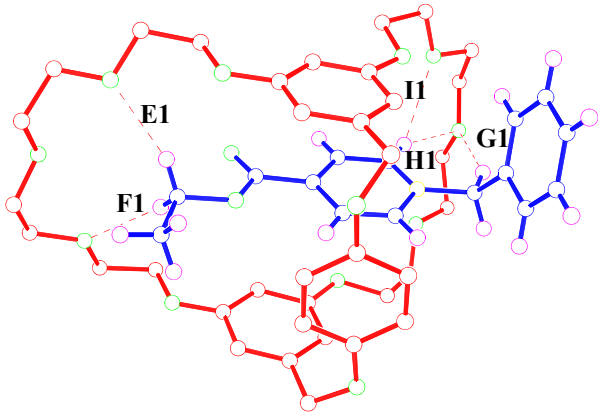

Figure 10. Ball-stick view of [2]pseudorotaxane **1f•3a**. **1f** is red and **3a** is blue. The PF_6 counterion, solvent molecules, and the hydrogens on **1f** were omitted for clarity. Oxygens are green, nitrogens are yellow, and hydrogens are magenta. Hydrogen-bond parameters: C···O distances (Å), H···O distances (Å), C-H···O angles (deg) **E1**, 3.36, 2.41, 162; **F1**, 3.29, 2.42, 146; **G1**, 3.54, 2.63, 152; **H1**, 3.26, 2.36, 158; **I1**, 3.15, 2.52, 123. Face-to-face π-stacking parameters: centroid-centroid distances (Å) 3.91, 4.39; ring plane/ring plane inclinations (deg): 2.8, 2.3. Edge-to-face π-stacking parameters: hydrogen-centroid distance (Å) 2.75, carbon-centroid distance (Å) 3.53, carbon-hydrogen-centroid angle (deg): 140.

14.3. CONCLUSIONS

In summary, we demonstrated that threaded structures (pseudorotaxanes) can be efficiently prepared based on the new cryptand/monopyridinium recognition motif. Though monopyridinium salts do not complex these cryptands as strongly as paraquat derivatives, they have better solubility in organic solvents than paraquat derivatives. Once interlocked structures (rotaxanes or catenanes) based on monopyridinium salts are made, they have the potential to be reduced in order to prepare neutral interlocked structures.[23] Also the starting materials to make monopyridinium salts are much cheaper than those for preparing paraquat derivatives. Currently we are focusing on using this new recognition motif to construct novel supramolecular systems.

14.4. ACKNOWLEDGEMENTS

This work was supported by the National Science Foundation (DMR0097126) and the Petroleum Research Fund (40223-AC7). The purchase of the diffractometer Xcalibur2 (VPI&SU) was also supported by the National Science Foundation (CHE-131128).

15.5. EXPERIMENTAL SECTION

General Procedures. All solvents were HPLC or GC grade. NMR solvents were bought from Cambridge Isotope Laboratories and used as received. The NMR spectra were recorded on a Varian Unity or Inova Instrument. Low-resolution electrospray ionization mass spectroscopy of all pseudorotaxanes in 4:1 acetonitrile:chloroform were carried out on a local TSQ Finnigan LC/MS/MS instrument. Melting points were taken in capillary tubes and are uncorrected. Elemental analyses were performed by Atlantic Microlabs of Norcross, GA. X-Ray diffraction data of cryptand **1b** and pseudorotaxanes **1a•3a**, **1b•3a**, **1e•3a**, and **1f•3a** were collected on an Oxford Diffraction XCalibur2™ diffractometer equipped with the Enhance X-ray Source™ (MoKα radiation; λ = 0.71073 Å) and a Sapphire 2™ CCD detector by the phi and omega scan method. For every data

collection, the chosen crystal was mounted on a nylon CryoLoop™ (Hampton Research) with Krytox® Oil (DuPont). The data collection routine, unit cell refinement, and data processing were carried out with the program CrysAlis.[24] X-Ray diffraction experiments of pseudorotaxanes **1c•3a** and **1d•3a** were carried out on a Bruker SMART CCD diffractometer equipped with MoK_α radiation (λ = 0.71073 Å) and a graphite monochromator by the phi and omega scan method.

4-Carbethoxy-1-Benzylpyridinium Hexafluorophosphate (3a). To a 50 mL three-necked round bottom flask equipped with a magnetic stirrer and a condenser were added 3.42 g (20.0 mmol) of benzyl bromide and 10 mL acetonitrile. To this solution was added a solution of ethyl isonicotinate (1.51 g, 10.0 mmol) in 10 mL acetone and the mixture was stirred at reflux for 48 hours. The reaction mixture was cooled to room temperature and the precipitate was filtered. The solid was boiled in $CHCl_3$ and filtered. This solid was dissolved in a minimum volume of deionized water. To this solution was added NH_4PF_6 until no further precipitation was observed. The precipitate was filtered and recrystallized from deionized water three times to afford **3a** as white crystals, 3.21 g (83%), m.p. 173.9-174.6 °C. ^{1}H NMR (400 MHz, acetone-d_6, 22 °C): δ = 1.45 (t, J = 7.2 Hz, 3H), 4.54 (q, J = 7.2 Hz, 2H), 6.23 (s, 2H), 7.52-7.56 (m, 3H), 7.66-7.70 (m, 2H), 8.73 (d, J = 6.8 Hz, 2H), 9.51 (d, J = 6.8 Hz, 2H); elemental analysis calcd for $C_{15}H_{16}O_2N_1P_1F_6$: C, 46.50; H, 4.17; N, 3.62; Found : C, 46.70, 46.53; H, 4.03, 3.99; N, 3.66, 3.74.

4-Carbethoxy-1-Methylpyridinium Hexafluorophosphate (3b). **3b**, prepared in a similar way as **3a**, was obtained as white crystals (81%), m.p. 127.8-128.5 °C. ^{1}H NMR (400 MHz, acetone-d_6, 22 °C): δ = 1.46 (t, J = 7.2 Hz, 3H), 4.55 (q, J = 7.2 Hz, 2H), 4.78 (s, 3H), 8.70 (d, J = 6.8 Hz, 2H), 9.37 (d, J = 6.8 Hz, 2H); elemental analysis calcd for $C_9H_{12}O_2N_1P_1F_6$: C, 34.72; H, 3.89; N, 4.50; Found : C, 34.77, 34.75; H, 3.84, 3.73; N, 4.55, 4.47.

Complexation Studies by Proton NMR. All solutions were prepared as follows. Precisely weighed amounts of dried hosts and guests were added into separate screw cap vials. The solvent was added with to-deliver volumetric pipets. Then specific volumes of each fresh solution were mixed to yield the desired concentrations. For example, in order

to make three solutions, 0.500 mM **1a**/1.00 mM **3a,** 0.500 mM **1a**/2.00 mM **3a**, and 0.500 mM **1a**/5.00 mM **3a**, a 1.00 mM solution of **1a** was made first by adding 5.00 mL acetone-d_6 with a 5.00 mL to-deliver pipette into a screw cap vial containing 3.63 mg (0.00500 mmol) of **1a**. Then 0.300 mL of this solution was added with a 0.300 mL to-deliver pipet to each of three vials that contained 0.300 mL of 2.00 mM, 0.300 mL of 4.00 mM, and 0.300 mL of 10.0 mM of **3a** separately. ^{1}H NMR data were collected on a temperature controlled spectrometer. Acetone-d_6 and 1:1 acetone-d_6:chloroform-*d* were chosen as the NMR solvents because all compounds used here have relatively good solubilities in them.

Determination of Association Constants ($K_{a,\mathbf{1}\bullet\mathbf{3}}$) for [2]Pseudorotaxanes 1•3. ^{1}H NMR characterizations were done on solutions with constant $[\mathbf{1}]_0$ and varied $[\mathbf{3}]_0$. Based on these NMR data, $\Delta_{0,\mathbf{1}}$, the difference in δ values for H_1 of **1** in the uncomplexed and fully complexed species, was determined by the extrapolation of a plot of $\Delta = \delta - \delta_u$ vs. $1/[\mathbf{3}]_0$ in the high initial concentration range of **3**. The resultant $\Delta_{0,\mathbf{1}}$ values for **1a•3a**, **1a•3b**, **1a•3c**, **1b•3a**, **1c•3a**, **1d•3a**, **1e•3a**, and **1f•3a** were 0.429 (acetone) and 0.450 ppm (1:1 acetone:chloroform), 0.206 (acetone) and 0.277 ppm (1:1 acetone:chloroform), 0.185 (acetone) and 0.242 ppm (1:1 acetone:chloroform), 0.117 ppm (1:1 acetone:chloroform), 0.144 ppm (1:1 acetone:chloroform), 0.134 ppm (1:1 acetone:chloroform), 0.283 ppm (1:1 acetone:chloroform), and 0.503 ppm (1:1 acetone:chloroform), respectively. Then $K_{a,\mathbf{1}\bullet\mathbf{3}}$ values at different $[\mathbf{1}]_0$ and $[\mathbf{3}]_0$ were calculated from $K_{a,\mathbf{1}\bullet\mathbf{3}} = (\Delta_{\mathbf{1}}/\Delta_{0,\mathbf{1}})/\{1 - (\Delta_{\mathbf{1}}/\Delta_{0,\mathbf{1}})\}\{[\mathbf{3}]_0 - (\Delta_{\mathbf{1}}/\Delta_{0,\mathbf{1}})[\mathbf{1}]_0\}$. The values and errors of $K_{a,\mathbf{1}\bullet\mathbf{3}}$ in Table 1 are mean values and standard derivations of $K_{a,\mathbf{1}\bullet\mathbf{3}}$ values at four or five points with different $[\mathbf{1}]_0$ and $[\mathbf{3}]_0$.

X-ray Analysis of 1a•3a (Figure 5). The structure was solved by direct methods using SIR-92[25] and refined using SHELXTL NT.[26] The asymmetric unit of the structural model comprises 2 crystallographically independent host/guest complexes plus an additional half a guest salt and 5.38 water molecules. After locating the main residues and the waters within and around their periphery of the residues, additional residual electron density that was presumably evaporated/disordered solvent could not be modeled successfully. Consequently, the SQUEEZE[27] subroutine of the program package

PLATON[28] was used to identify potential solvent/void regions and subtract any electron density contribution in this region from the structure factors. A total of 639.4 $Å^3$ void space was identified (9.7% of total cell volume), but electron density totaling only 3 e^- was subtracted. Presumably the strong non-bonding interactions between the host and guest allowed the solvent to evaporate without the sample losing crystallinity. The final refinement model involved anisotropic displacement parameters for non-hydrogen atoms, except the disordered atoms in the host molecules. A riding model was used for all hydrogen atoms. No hydrogen positions were located or calculated for the water molecules. Data were collected on a Oxford Diffraction Sapphire 2 CCD diffractometer by the omega scan method in a range $1.4^o \leq \theta \leq 19.8^o$. Crystal data: block, yellow, 0.34 × 0.22 × 0.12 mm^3, $C_{54.75}H_{79.373}F_{7.50}N_{1.25}O_{20.19}P_{1.25}$, FW = 1259.33, triclinic, space group P-1, a = 10.8768(10)**,** b = 23.3640(18), c = 27.605(3) Å, α = 103.533(7), β = 100.307(8)°, γ = 97.849(7), V = 6592.6(10) $Å^3$, Z = 4, D_c = 1.269 g cm^{-3}, T = 100 K, μ = 1.37 cm^{-1}, 32144 measured reflections, 23206 independent reflections [R(int) = 0.0540], 1646 parameters, 164 restraints, F(000) = 2658, R_1 = 0.2109, wR_2 = 0.2957 (all data), R_1 = 0.0981, wR_2 = 0.2387 using 8786 reflections with $I > 2\sigma(I)$, maximum residual density 0.696 e•$Å^{-3}$, and goodness-of-fit (F^2) = 0.966.

X-ray Analysis of 1b (Figure 7a). The structure was solved by the direct methods using SIR-92 and refined by full-matrix least squares using Crystals.[29] Nonhydrogen atoms were treated anisotropically and hydrogen atoms were placed in calculated positions. Crystal data: prism, colorless, 0.32 × 0.15 × 0.10 mm^3, $C_{30}H_{44}O_{13}$, FW = 612.67, triclinic, space group P-1, a = 11.1123(11)**,** b = 12.0045(15), c = 13.1472(18) Å, α = 68.838(12)°, β = 75.51(1)°, γ = 67.07(1)°, V = 1494.0(3) $Å^3$, Z = 2, D_c = 1.362 g cm^{-3}, T = 100K, μ = 1.06 cm^{-1}, 16286 measured reflections, 9297 independent reflections [R(int) = 0.02], 389 parameters, F(000) = 656, R_1 = 0.0578, wR_2 = 0.0543 (all data), R_1 = 0.0497, wR_2 = 0.0533 [$I > 1\sigma(I)$], maximum residual density 0.40 e•$Å^{-3}$, and goodness-of-fit (F^2) = 1.1248.

X-ray Analysis of 1b•3a (Figure 7b). The structure was solved by direct methods and refined using the SHELXTL NT. The asymmetric unit of the structure comprises one crystallographically independent host-guest complex. The final refinement

model involved anisotropic displacement parameters for non-hydrogen atoms and a riding model for all hydrogen atoms. Crystal data: plate, yellow, 0.058 × 0.148 × 0.244 mm^3, $C_{45}H_{58}F_6NO_{14}P$, FW = 981.89, monoclinic, space group $P2_1/n$, a = 10.1411(15), b = 21.048(4), c = 21.152(3) Å, β = 93.236(12)°, V = 4507.7(12) $Å^3$, Z = 4, D_c = 1.447 g cm^{-3}, T = 100K, μ = 1.55 cm^{-1}, 22096 measured reflections, 7972 independent reflections [R(int) = 0.0709], 605 parameters, F(000) = 2064, R_1 = 0.1326, wR_2 = 0.0966 (all data), R_1 = 0.0613, wR_2 = 0.0777 [$I > 2\sigma(I)$], maximum residual density 0.316 e•$Å^{-3}$, and goodness-of-fit (F^2) = 0.986.

X-ray Analysis of 1c•3a (Figure 6). SADABS[30] absorption corrections were applied. The structure was solved by direct methods and refined by full-matrix least squares procedure on F^2 using the SHELXTL. Non-hydrogen atoms were refined with anisotropic displacement coefficients, and hydrogen atoms were treated as idealized contributions. Crystal data: blade, colorless, 0.10 × 0.10 × 0.03 mm^3, $C_{52}H_{61}F_6N_2O_{19}P$, FW = 1163.00, monoclinic, space group $P2_1/n$, a = 14.742(3), b = 20.650(3), c = 19.244(3) Å, β = 104.346(3)°, V = 5675.5(17) $Å^3$, Z = 4, D_c = 1.361 g cm^{-3}, T = 208(2) K, μ = 1.42 cm^{-1}, 29441 measured reflections, 7401 independent reflections [R(int) = 0.0685], 721 parameters, 0 restraints, F(000) = 2432, R1 = 0.1534, wR2 = 0.3107 (all data), R1 = 0.1076, wR2 = 0.2779 using 4741 reflections with $I > 2\sigma(I)$, maximum residual density 1.531 e•$Å^{-3}$, and goodness-of-fit (F^2) = 1.068.

X-ray Analysis of 1d•3a (Figure 8a). The structure was solved by direct methods and refined by full-matrix least squares procedure on F^2 using the SHELXTL. Non-hydrogen atoms were refined with anisotropic displacement coefficients, and hydrogen atoms were treated as idealized contributions. Crystal data: plate, pale yellow, 0.30 × 0.30 × 0.20 mm^3, $C_{57.50}H_{76}F_6NO_{16}P$, FW = 1182.16, triclinic, space group P-1, a = 11.0155(9), b = 13.3102(11), c = 21.2726(18) Å, α = 89.0340(10)°, β = 81.7310(10)°, γ = 68.0420(10)°, V = 2860.3(4) $Å^3$, Z = 2, D_c = 1.373 g cm^{-3}, T = 100 K, μ = 1.38 cm^{-1}, 22605 measured reflections, 11128 independent reflections [R(int) = 0.0223], 712 parameters, F(000) = 1250, R_1 = 0.0674, wR_2 = 0.1520 (all data), R_1 = 0.0533, wR_2 = 0.1436 [$I > 2\sigma(I)$], maximum residual density 1.592 e•$Å^{-3}$, and goodness-of-fit (F^2) = 1.090.

X-ray Analysis of 1d•3a (Figure 8b). SADABS absorption corrections were applied. The structure was solved by direct methods and refined by full-matrix least squares procedure on F^2 using the SHELXTL. Non-hydrogen atoms were refined with anisotropic displacement coefficients, and hydrogen atoms were treated as idealized contributions. Crystal data: plate, pale yellow, 0.30 × 0.25 × 0.20 mm^3, $C_{55}H_{70}F_6NO_{16}P$, *FW* = 1146.09, monoclinic, space group $P2_1/c$, a = 10.661(4), b = 29.733(10), c = 17.235(6) Å, β = 97.731(6)°, V = 5413(3) $Å^3$, Z = 4, D_c = 1.406 g cm^{-3}, T = 100K, μ = 1.43 cm^{-1}, 11150 measured reflections, 7411 independent reflections [R(int) = 0.0370], 716 parameters, F(000) = 2416, R_1 = 0.0715, wR_2 = 0.1025 (all data), R_1 = 0.0438, wR_2 = 0.0919 [$I > 2\sigma(I)$], maximum residual density 0.353 e•$Å^{-3}$, and goodness-of-fit (F^2) = 0.983.

X-ray Analysis of 1e•3a (Figure 9). The structure was solved by direct methods and refined using the SHELXTL NT. The asymmetric unit of the structure comprises one crystallographically independent host-guest complex. The final refinement model involved anisotropic displacement parameters for non-hydrogen atoms and a riding model for all hydrogen atoms. Crystal data: block, pale yellow, 0.275 × 0.327 × 0.356 mm^3, $C_{50}H_{61}F_6N_2O_{14}P$, *FW* = 1058.98, monoclinic, space group $P2_1/c$, a = 23.9952(17), b = 13.4583(10), c = 16.0394(12) Å, β = 105.273(6)°, V = 4996.7(6) $Å^3$, Z = 4, D_c = 1.408 g cm^{-3}, T = 100K, μ = 1.46 cm^{-1}, 54370 measured reflections, 14618 independent reflections [R(int) = 0.0288], 659 parameters, F(000) = 2224, R_1 = 0.0647, wR_2 = 0.1196 (all data), R_1 = 0.0549, wR_2 = 0.1146 [$I > 2\sigma(I)$], maximum residual density 0.307 e•$Å^{-3}$, and goodness-of-fit (F^2) = 1.195.

X-ray Analysis of 1f•3a (Figure 10). The structure was solved by direct methods and refined using the SHELXTL NT. The asymmetric unit of the structure comprises one crystallographically independent host-guest complex. The final refinement model involved anisotropic displacement parameters for non-hydrogen atoms and a riding model for all hydrogen atoms. Crystal data: needle, pale yellow, 0.14 × 0.17 × 0.56 mm^3, $C_{54}H_{68}F_6NO_{15}P$, *FW* = 1116.06, monoclinic, space group $P2_1/c$, a = 11.377(2), b = 18.145(3), c = 27.106(5) Å, β = 99.856(17)°, V = 5513.2(18) $Å^3$, Z = 4, D_c = 1.345 g cm^{-3}, T = 100K, μ = 1.37 cm^{-1}, 30997 measured reflections, 12702 independent reflections

[R(int) = 0.0330], 697 parameters, $F(000)$ = 2352, R_1 = 0.1069, wR_2 = 0.1907 (all data), R_1 = 0.0647, wR_2 = 0.1647 [$I > 2\sigma(I)$], maximum residual density 0.583 e•Å^{-3}, and goodness-of-fit (F^2) = 1.112.

14.6. SUPPORTING INFORMATION

*Electrospray mass spectrum of a solution of **1a** and **3b** in a mixture of acetonitrile and chloroform (4:1).*

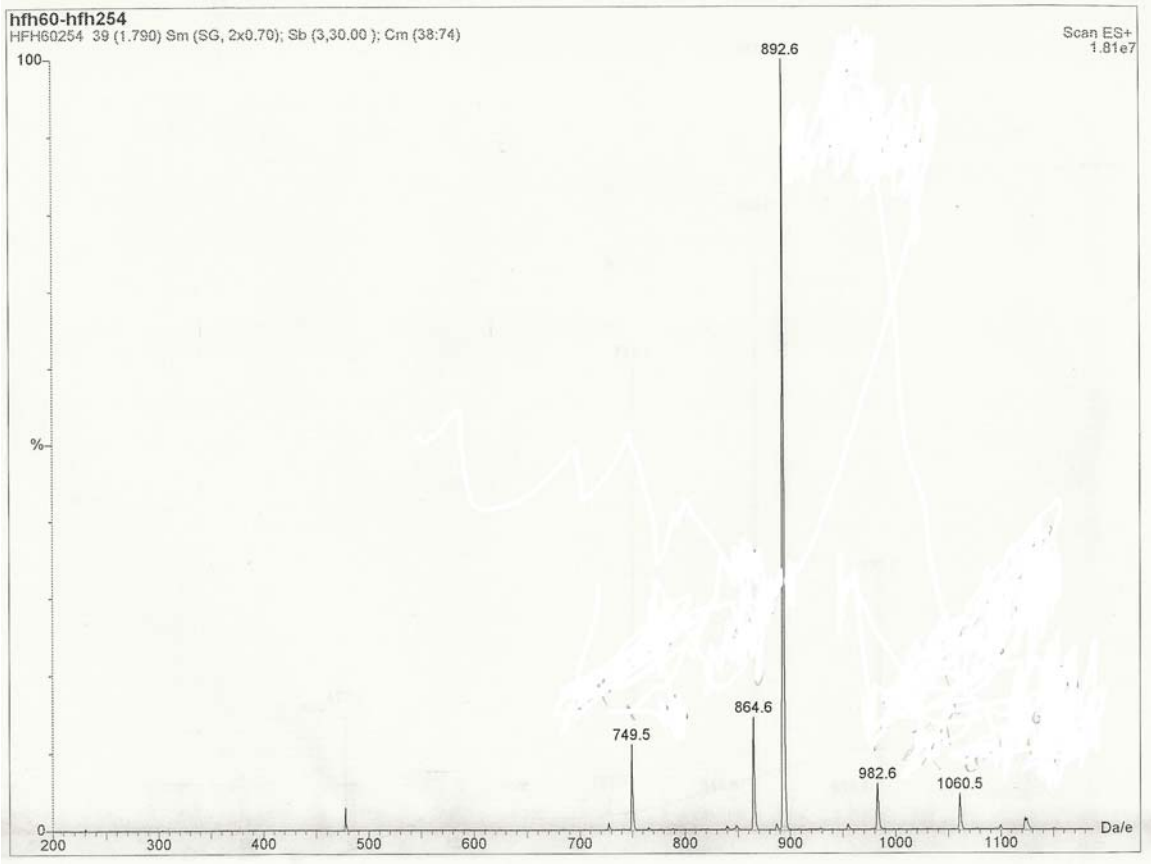

Assignments of main peaks: *m*/*z* 1060.5 [**1a•3b** + Na]$^+$, 982.6 [**1a•3b** + Li – $HOCH_2CH_2OH$]$^+$, 892.6 [**1a•3b** – PF_6]$^+$, 864.6 [**1a•3b** – PF_6 – C_2H_4]$^+$, and 749.5 [**1a** + Na]$^+$.

*Electrospray mass spectrum of a solution of **1a** and **3c** in a mixture of acetonitrile and chloroform (4:1).*

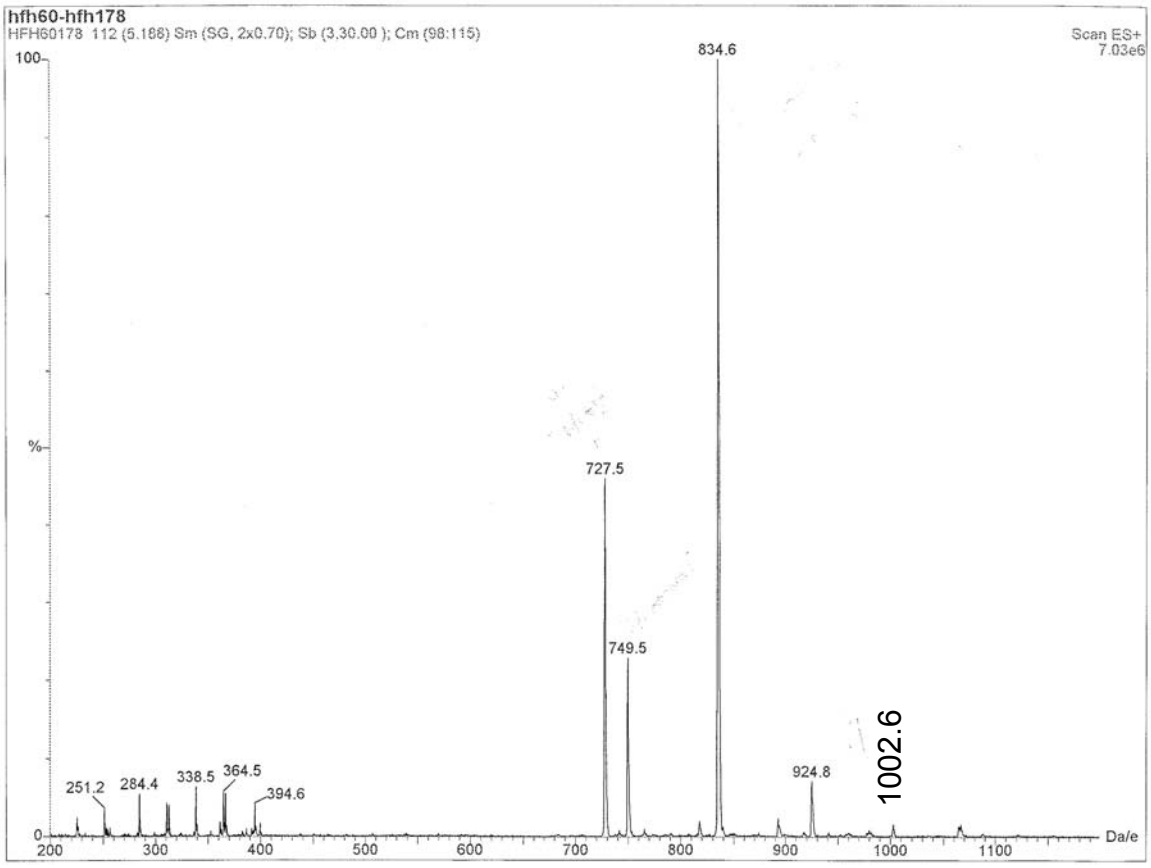

Assignments of main peaks: *m/z* 1002.6 [**1a•3c** + Na]$^+$, 924.8 [**1a•3c** + Li – $HOCH_2CH_2OH$]$^+$, 834.6 [**1a•3c** – PF_6]$^+$, 749.5 [**1a** + Na]$^+$, and 727.5 [**1a** + H]$^+$.

*Electrospray mass spectrum of a solution of **1c** and **3a** in a mixture of acetonitrile and chloroform (4:1).*

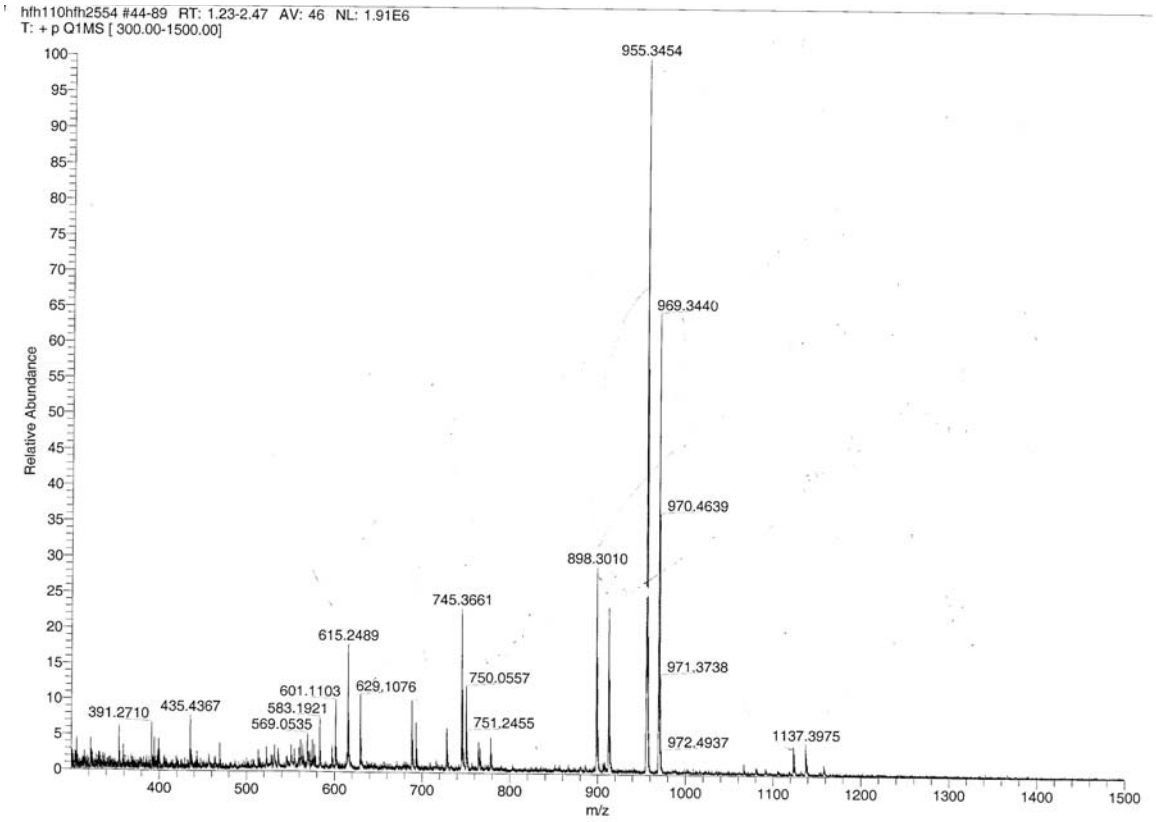

Assignments of main peaks: *m/z* 1137.4 [**1c•3a** + Na]$^+$, 1123.3 [**1c•3a** + Na – CH_3 + H]$^+$, 969.3 [**1c•3a** – PF_6]$^+$, 955.3 [**1c•3a** – PF_6 – CH_3 + H]$^+$, 912.3 [**1c•3a** – HPF_6 – C_6H_6 + Na – H]$^+$, 898.3 [**1c•3a** – PF_6 – C_6H_6 + Li]$^+$, 750.1 [**1c** + Na]$^+$, 745.4 [**1c** + H_2O]$^+$, 629.5 [**3a**$_2$ – PF_6]$^+$, 615.2 [**3a**$_2$ – PF_6 – CH_3 + H]$^+$, and 601.1 [**3a**$_2$ – PF_6 – C_2H_5 + H]$^+$.

*Electrospray mass spectrum of a solution of **1d** and **3a** in a mixture of acetonitrile and chloroform (4:1).*

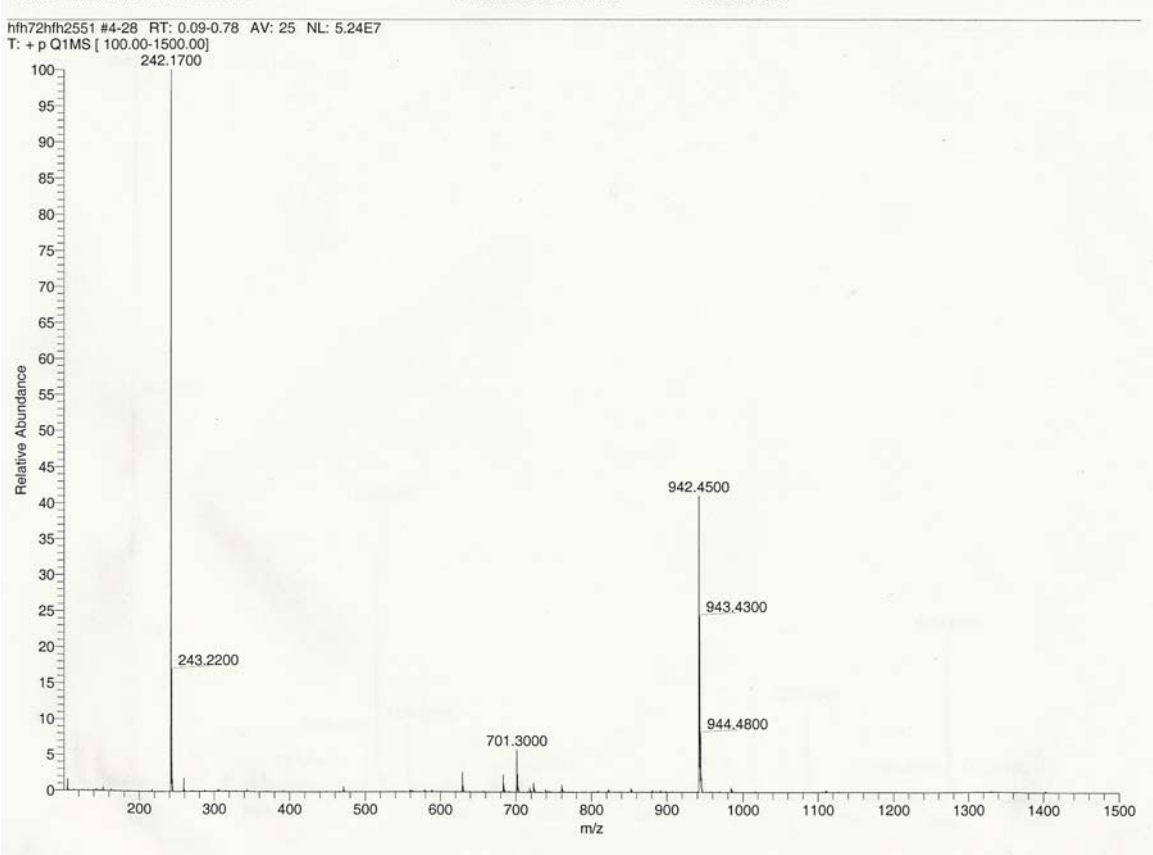

Assignments of main peaks: *m*/*z* 942.5 [**1d•3a** – PF_6]$^+$, 701.3 [**1d** + H]$^+$, and 242.2 [**3a** – PF_6]$^+$.

*Electrospray mass spectrum of a solution of **1e** and **3a** in a mixture of acetonitrile and chloroform (4:1).*

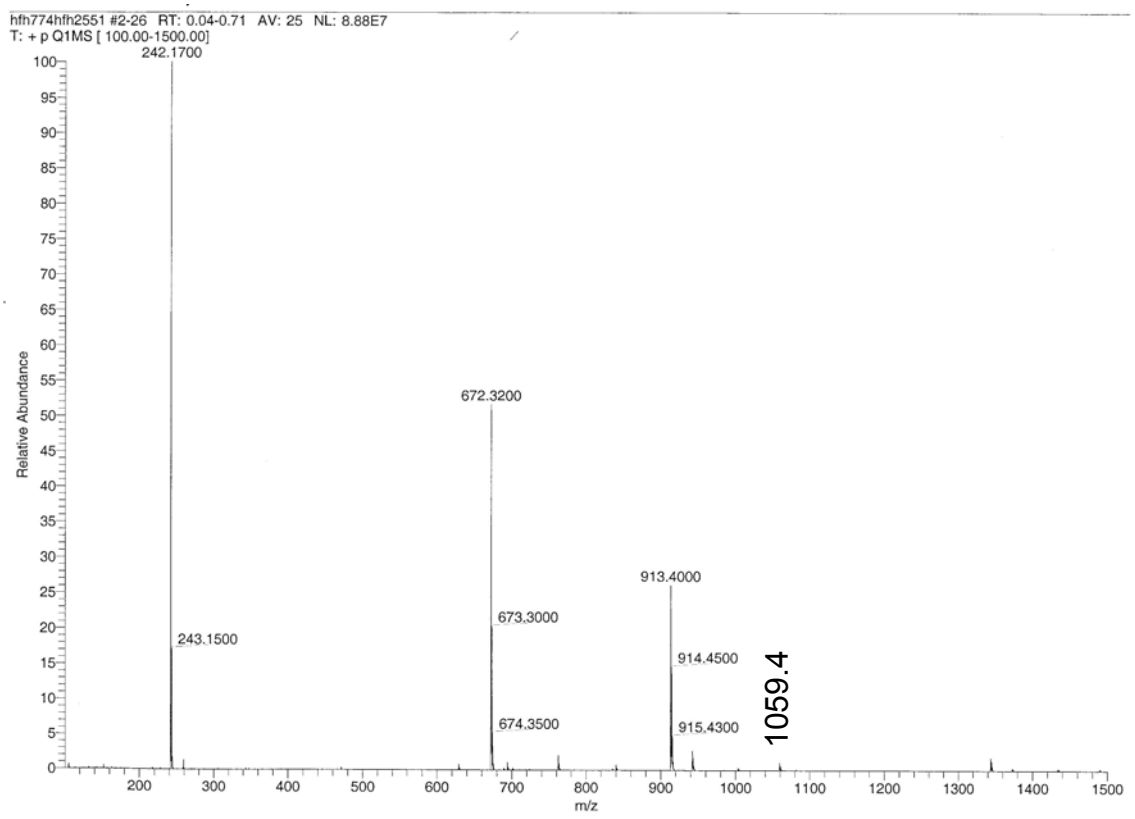

Assignments of main peaks: *m/z* 1059.4 [**1e•3a** + H]$^+$, 913.4 [**1e•3a** – PF_6]$^+$, 672.3 [**1e** + H]$^+$, and 242.2 [**3a** – PF_6]$^+$.

REFERENCES

1. Gibson, H. W. in *Large Ring Molecules*; Semlyen, J. A. Ed.; John Wiley & Sons: New York, 1996; pp. 191-262. Philp, D.; Stoddart, J. F. *Angew. Chem. Int. Ed. Engl.* **1996**, *35*, 1155-1196. Raymo, F. M.; Stoddart, J. F. *Chem. Rev.* **1999**, *99*, 1643-1664. *Catenanes, Rotaxanes and Knots* Sauvage, J.–P.; Dietrich-Buchecker, C. O. Eds.; Wiley-VCH: Weinheim, 1999. Mahan E.; Gibson H. W. in *Cyclic Polymers, 2nd ed*.; Semlyen, A. J. Ed.; Kluwer Publishers: Dordrecht, 2000; pp 415-560. Hubin, T. J.; Busch, D. H. *Coord. Chem. Rev.* **2000**, *200-202*, 5-52. Panova, I. G.; Topchieva, I. N. *Russ. Chem. Rev.* **2001**, *70*, 23-44.
2. Allwood, B. L.; Spencer, N.; Shahriari-Zavareh, H.; Stoddart, J. F.; Williams, D. J. *J. Chem. Soc., Chem. Commun.* **1987**, 1064-1066. Ashton, P. R.; Philp, D.; Reddington, M. V.; Slawin, A. M. Z.; Spencer, N.; Stoddart, J. F.; Williams, D. J. *J. Chem. Soc., Chem. Commun.* **1991**, 1680-1683. Huang, F.; Jones, J. W.; Slebodnick, C.; Gibson, H. W. *J. Am. Chem. Soc.* **2003**, *125*, 14458-14464.
3. (a) Fyfe, M. C. T.; Stoddart, J. F. *Adv. Supramol. Chem.* **1999**, *5*, 1-53. (b) Bryant, W. S.; Guzei, I.; Rheingold, A. L.; Gibson, H. W. *Org. Lett.* **1999**, *1*, 47-50. (c) Huang, F.; Zakharov, L. N.; Rheingold, A. L.; Jones, J. W.; Gibson, H. W. *Chem. Commun.* **2003**, 2122-2123. (d) Jones, J. W.; Gibson, H. W. *J. Am. Chem. Soc.* **2003**, *125*, 7001-7004. (e) Hung, W.-C.; Liao, K.-S.; Liu, Y.-H.; Peng, S.-M.; Chiu, S.-H. *Org. Lett.* **2004**, *6*, 4183-4186. (f) Lowe, J. N.; Fulton, D. A.; Chiu, S.-H.; Elizarov, A. M.; Cantrill, S. J.; Rowan, S. J.; Stoddart, J. F. *J. Org. Chem.* **2004**, *69*, 4390-4402.
4. Vögtle, F.; Hunten, A.; Vogel, E.; Buschbeck, S.; Safarowsky, O.; Recker, J.; Parham, A.-H.; Knott, M.; Müller, W. M.; Muller, U.; Okamoto, Y.; Kubota, T.; Lindner, W.; Francotte, E.; Grimme, S. *Angew. Chem. Int. Ed.* **2001**, *40*, 2468-2471. Hunter, C. A.; Low, C. M. R.; Packer, M. J.; Spey, S. E.; Vinter, J. G.; Vysotsky, M. O.; Zonta, C. *Angew. Chem. Int. Ed.* **2001**, *40*, 2678-2682. Leigh, D. A.; Wong, J. K. Y.; Dehez, F.; Zerbetto, F. *Nature* **2003**, *424*, 174-179. Schalley, C. A.; Reckien, W.; Peyerimhoff, S.; Baytekin, B.; Vögtle, F. *Chem. Eur. J.* **2004**,

10, 4777-4789. Leigh, D. A.; Venturini, A.; Wilson, A. J.; Wong, J. K. Y.; Zerbetto, F. *Chem. Eur. J.* **2004**, *10*, 4960-4969. Hernández, J. V.; Kay, E. R.; Leigh, D. A. *Science* **2004**, *306*, 1532-1537.

5. Odell, B.; Reddington, M. V.; Slawin, A. M. Z.; Spencer, N.; Stoddart, J. F.; Williams, D. J. *Angew. Chem. Int. Ed. Engl.* **1988**, *27*, 1547-1550. Liu, Y.; Flood, A. H.; Stoddart, J. F. *J. Am. Chem. Soc.* **2004**, *126*, 9150-9151. Deng, W.-Q.; Muller, R. P.; Goddard, W. A., III. *J. Am. Chem. Soc.* **2004**, *126*, 13562-13563.
6. Ogino, H. *J. Am. Chem. Soc.* **1981**, *103*, 1303-1304. Yamanari, K.; Y. Shimura, *Chem. Lett.* **1982**, *12*, 1959-1962. Gonzalez, B.; Cuadrado, I.; Alonso, B.; Casado, C. M.; Moran, M.; Kaifer, A. E. *Organometallics* **2002**, *21*, 3544-3551. Pang, Y.; Ritter, H.; Tabatabai, M. *Macromolecules* **2003**, *36,* 7090-7093. Okada, M.; Harada, A. *Org. Lett.* **2004**, *6*, 361-364.
7. Arduini, A.; Ferdani, R.; Pochini, A.; Secchi, A.; Ugozzoli, F. *Angew. Chem. Int. Ed.* **2000**, *39*, 3453-3456. Arduini, A.; Calzavacca, F.; Pochini, A.; Secchi, A. *Chem. Eur. J.* **2003**, *9*, 793-799.
8. (a) Rowan, A. E.; Aarts, P. P. M.; Koutstaal, K. W. M. *Chem. Commun.* **1998**, 611-612. (b) Gunter, M. J.; Jeynes, T. P.; Johnston, M. R.; Turner, P.; Chen, Z. *J. Chem. Soc., Perkin. 1.* **1998**, 1945-1957. (c) Elemans, J. A. A. W.; Claase, M. B.; Aarts, P. P. M.; Rowan, A. E.; Schenning, A. P. H. J.; Nolte, R. J. M. *J. Org. Chem.* **1999**, *64,* 7009-7016. (d) Bryant, W. S.; Jones, J. W.; Mason, P. E.; Guzei, I. A.; Rheingold, A. L.; Nagvekar, D. S.; Gibson, H. W. *Org. Lett.* **1999**, *1*, 1001-1004. (e) Huang, F.; Fronczek, F. R.; Gibson, H. W. *J. Am. Chem. Soc.* **2003**, *125*, 9272-9273. (f) Huang, F.; Gibson, H. W.; Bryant, W. S.; Nagvekar, D. S.; Fronczek, F. R. *J. Am. Chem. Soc.* **2003**, *125*, 9367-9371. (g) Huang, F.; Zhou, L.; Jones, J. W.; Gibson, H. W.; Ashraf-Khorassani, M. *Chem. Commun.* **2004**, 2670-2671. (h) Huang, F.; Switek, K. A.; Zakharov, L. N.; Fronczek, F. R.; Slebodnick, C.; Lam, M.; Golen, J. A.; Bryant, W. S.; Mason, P.; Rheingold, A. L.; Ashraf-Khorassani, M.; Gibson, H. W. *J. Org. Chem.* **2005**, In press.
9. Loeb, S. J.; Wisner, J. A. *Angew. Chem. Int. Ed.* **1998**, *37*, 2838-2840. Hubbard, A. L.; Davidson, G. J. E.; Patel, R. H.; Wisner, J. A.; Loeb, S. J. *Chem. Commun.*

2004, 138-139.

10. Kim, H.-J.; Jeon, W. S.; Ko, Y. H.; Kim, K. *Proc. Natl. Acad. Sci. U. S. A.* **2002**, *99*, 5007-5011. Choi, S. W.; Lee, J. W.; Ko, Y. H.; Kim, K. *Macromolecules* **2002**, *35*, 3526-3531. Tuncel, D.; Steinke, J. H. G. *Chem. Comm.* **2002**, 496-497. Tuncel, D.; Steinke, J. H. G. *Macromolecules* **2004**, *37*, 288-302. Sindelar, V.; Moon, K.; Kaifer, A. E. *Org. Lett.* **2004**, *6*, 2665-2668.
11. Dietrich-Buchecker, C.; Colasson, B.; Fujita, M.; Hori, A.; Geum, N.; Sakamoto, S.; Yamaguchi, K.; Sauvage, J.-P. *J. Am. Chem. Soc.* **2003**, *125*, 5717-5725. Flamigni, L.; Talarico, A. M.; Chambron, J.-C.; Heitz, V.; Linke, M.; Fujita, N.; Sauvage, J.-P. *Chem. Eur. J.* **2004**, *10*, 2689-2699. Kwan, P. H.; MacLachlan, M. J.; Swager, T. M. *J. Am. Chem. Soc.* **2004**, *126*, 8638-8639. Perret-Aebi, L.-E.; von Zelewsky, A.; Dietrich-Buchecker, C.; Sauvage, J.-P. *Angew. Chem. Int. Ed.* **2004**, *43*, 4482-4485.
12. (a) Simmons, H. E.; Park, C. H. *J. Am. Chem. Soc.* **1968**, *90*, 2428-2429; 2429-2431; 2431-2432. (b) Reviews: Dietrich, B. in *Comprehensive Supramolecular Chemistry, Vol. 1*; Lehn, J.-M., Atwood, J. L., Davies, J. E. D., McNicol, D. D., Vogtle, F., Eds.; Pergamon Press: Oxford, 1996; pp 153-211. Lucht, B. L.; Collum, D. B. *Acc. Chem. Res.* **1999**, *32*, 1035-1042. Reed, C. A.; Bolskar, R. D. *Chem. Rev.* **2000**, *100*, 1075-1120. Kaes, C.; Katz, A.; Hosseini, M. W. *Chem. Rev.* **2000**, *100*, 3553-3590.
13. Supramolecular cryptands have been referred to as "pseudocryptands". For the first such reference see: Nabeshima, T.; Inaba, T.; Sagae, T.; Furukawa, N. *Tetrahedron Lett.* **1990**, *31*, 3919-3922. For examples of recent references see: (a) Romain, H.; Florence, D.; Alain, M. *Chemistry* **2002**, *8*, 2438-2445. (b) Nabeshima, T.; Yoshihira, Y.; Saiki, T.; Akine, S.; Horn, E. *J. Am. Chem. Soc.* **2003**, *125*, 28-29. For a review see: Nabeshima, T.; Akine, S.; Saiki, T. *Rev. Heteroatom Chem.* **2000**, *22*, 219-239.
14. (a) Jones, J. W.; Zakharov, L. N.; Rheingold, A. L.; Gibson, H. W. *J. Am. Chem. Soc.* **2002**, *124*, 13378-13379. (b) Huang, F.; Zakharov, L. N.; Rheingold, A. L.; Jones, J. W.; Gibson, H. W. *Chem. Commun.* **2003**, 2122-2123. (c) Huang, F.;

Guzei, I. A.; Jones, J. W.; Gibson, H. W. *Chem. Commun.* **2005**, Advance Article, Feb. 5.

15. Niikura, K.; Bisson, A. P.; Anslyn, E. V. *J. Chem. Soc., Perkin Trans. 2.* **1999**, 1111-1114.
16. Hashizume, M.; Tobey, S.; Lynch, V. M.; Anslyn, E. V. Supramol. Chem. **2002**, *14*, 511-517.
17. Mahoney, J. M.; Beatty, A. M.; Smith, B. D. *J. Am. Chem. Soc.* **2001**, *123*, 5847-5848. Mahoney, J. M.; Stucker, K. A.; Jiang, H.; Carmichael, I.; Brinkmann, N. R.; Beatty, A. M.; Noll, B. C.; Smith, B. D. *J. Am. Chem. Soc.* **2005**, *127*, ACS ASAP.
18. Recent publications: (a) Yamada, D. S.; Misono, T.; Tsuzuki, S. *J. Am. Chem. Soc.* **2004**, *126*, 9682-9872. (b) Rashkin, M. J.; Hughes, R. M.; Calloway, N. T.; Waters, M. L. *J. Am. Chem. Soc.* **2004**, *126*, 13320-13325. (c) Zhao, D.; Fei, Z.; Geldbach, T. J.; Scopelliti, R.; Dyson, P. J. *J. Am. Chem. Soc.* **2004**, *126*, 15876-15882. (d) Pittelkow, M.; Christensen, J. B.; Meijer, E. W. *J. Polym. Sci., Pol. Chem.* **2004**, *42*, 3792-3799. (e) Vasilev, A.; Deligeorgiev, T.; Gadjev, N.; Drexhage, K.-H. *Dyes Pigment.* **2005**, *66*, 135-142. (f) Ilies, M. A.; Johnson, B. H.; Makori, F.; Miller, A.; Seitz, W. A.; Thompson, E. B.; Balaban, A. T. *Arch. Biochem. Biophys.* **2005**, *435*, 217-226. (g) Tsuji, K.; Nishimura, N.; Duan, X.-M.; Okada, S.; Oikawa, H.; Matsuda, H.; Nakanishi, H. *Bull. Chem. Soc. Jpn.* **2005**, *78*, 180-186. (h) Colilla, M.; Darder, M.; Aranda, P.; Ruiz-Hitzky, E. *Chem. Mat.* **2005**, *17*, 708-715.
19. Curiel, D.; Beer, P. D.; Paul, R. L.; Cowley, A.; Sambrook, M. R.; Szemes, F. *Chem. Comm.* **2004**, 1162-1163. Sambrook, M. R.; Beer, P. D.; Wisner, J. A.; Paul, R. L.; Cowley, A. R. *J. Am. Chem. Soc.* **2004**, *126*, 15364-15365.
20. Lämsä, M.; Huuskonen, J.; Rissanen, K.; Pursiainen, J. *Chem. Eur. J.* **1998**, *4*, 84-92.
21. Che, C. M.; Kwong, H. L.; Poon, C. K.; Yam, V. W. W. *J. Chem. Soc., Dalton Trans.: Inorg. Chem.* **1990**, 3215-3219.
22. Job, P. *Ann. Chim*. **1928**, *9*, 113-203.

23. Quaternized monopyridinium nuclei can be easily reduced by sodium borohydride to the neutral tetrahydro derivatives. See: *Pyridine and Its Derivatives*; Shaw, E. N.; Klingsberg, E. Eds.; Interscience: New York, 1960; Part 2, pp. 47-55. Paquette, L. A. *Modern Heterocyclic Chemistry*; W. A. Benjamin: New York, 1968; pp. 240-241.
24. CrysAlis v1.170, Oxford Diffraction: Wroclaw, Poland, 2002.
25. Burla, M. C.; Camalli, M.; Cascarano, G.; Giacovazzo, C.; Polidori, G.; Spagna, R.; Viterbo, D. *J. Appl. Cryst.* **1989,** *22,* 389-393.
26. Sheldrick, G. M. SHELXTL NT ver. 6.12; Bruker Analytical X-ray Systems, Inc.: Madison, WI, 2001.
27. Van der Sluis, P.; Spek, A. L. *Acta Crystollgr., Sect. A: Found. Crystallogr.* **1990**, *46*, 194-201.
28. Spek, A. L. *J. Appl. Cryst.* **2003,** *36*, 7-13.
29. Watkin, D. J.; Prout, C. K.; Carruthers, J. R.; Betteridge, P. W.; Cooper, R. I. CRYSTALS 2000, Issue 11. Chemical Crystallography Laboratory, University of Oxford, Oxford.
30. Sheldrick, G. M. (1998), SADABS (2.01), Bruker/Siemens Area Detector Absorption Correction Program, Bruker AXS, Madison, Wisconsin, USA.

TOC Graphic:

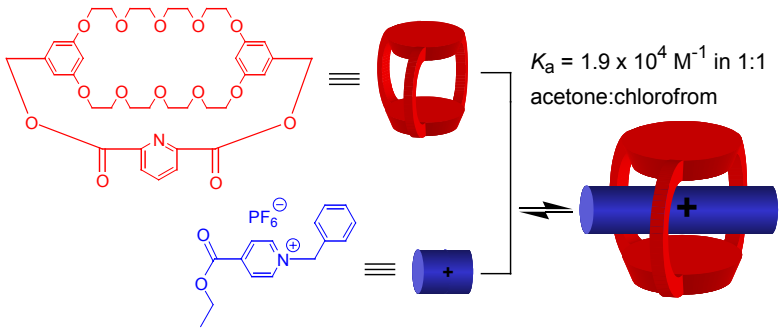

Abstract: The first cryptand/monopyridinium [2]pseudorotaxanes were successfully prepared from six bis(*m*-phenylene)-26-crown-8- or bis(*m*-phenylene)-32-crown-10-based cryptand hosts and monopyridinium guests based on the new cryptand/monopyridinium recognition motif. These pseudorotaxanes were studied by proton NMR spectroscopy, mass spectrometry, and X-ray analysis.